

Conf - 910864 - -5

11/29/91 JSD

SLAC-PUB--5674

DE92 003592

EVIDENCE FOR  $\rho(1600)$  FROM THE DECAY  $J/\psi \rightarrow \pi^- \pi^+ \pi^0$

Liang Ping Chen, Vanderbilt University, Nashville, TN 37235  
and

W. Dunwoodie, Stanford Linear Accelerator Center,  
Stanford University, Stanford, CA 94309

Representing the MARK III Collaboration

Abstract

Data from MARK III on the decay  $J/\psi \rightarrow \pi^- \pi^+ \pi^0$  are described in terms of amplitudes representing the sequential two-body decay processes  $J/\psi \rightarrow \rho \pi$ ,  $\rho \rightarrow \pi \pi$ . It is found that a complete description requires contributions from excited  $J^{PC} = 1^{--}$  states in addition to the dominant contribution from the  $\rho(770)$ . The characteristics of these additional states are discussed.

1. Introduction

The reaction

$$J/\psi \rightarrow \pi^- \pi^+ \pi^0 \quad (1)$$

accounts for  $\sim 1.5\%$  of all  $J/\psi$  decays.<sup>[1]</sup> Consequently, it is readily observed, and has been the subject of several previous studies.<sup>[1]</sup> However, in none of these studies has a detailed analysis of the final state been attempted. This paper describes the preliminary results from such an analysis in the full dimensionality of the three-pion final state, with particular emphasis on the parameters of the  $\rho(770)$  and the coupling of its excited states to the  $J/\psi$ .

\* This work was supported in part by the U. S. Department of Energy, under contracts DE-AC03-76SF00515, DE-AC02-76ER01195, DE-AC02-87ER40318, DE-AC03-81ER00650, DE-AM03-76SF00010, and by the National Science Foundation.

Presented by L.-P. Chen at the International Conference on Hadron Spectroscopy, College Park, Maryland, August 12-16, 1991

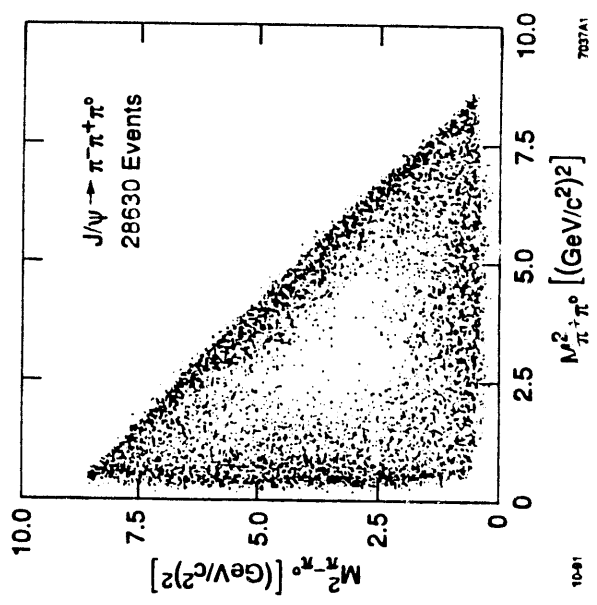


Figure 1. The Dalitz plot for reaction (1) (28630 events).

2. The Data Sample

The data on reaction (1) were acquired with the MARK III detector at the SPEAR storage ring at SLAC, and correspond to  $5.8 \times 10^6 J/\psi$  events. The procedures followed in defining the event sample are similar to those employed in previous MARK III analyses.<sup>[2-5]</sup> In particular, candidate two-prong events with at least two accompanying photons were subjected to four-constraint fits to the hypothesis  $J/\psi \rightarrow \pi^- \pi^+ \gamma \gamma$ . Events yielding a fit confidence level greater than  $10^{-2}$  were retained if the  $\gamma\gamma$  effective mass was in the range (85-185) MeV/c<sup>2</sup>. Surviving events were then subjected to a five-constraint fit to reaction (1) in order to improve the three-momentum resolution of the  $\pi^0$  and its daughter photons. Monte Carlo studies revealed that this sample still contained a significant contamination at low photon energy due to split-off photons associated with the charged pion tracks. This was removed by requiring that each final state photon have energy greater than 60 MeV and satisfy  $\cos\theta_\gamma \leq 0.98$ , where  $\theta_\gamma$  is the angle between the photon in question and the closer of the two charged pion tracks. The Dalitz plot

MASTER

DISTRIBUTION OF THIS DOCUMENT IS UNLIMITED

for the resulting sample of  $\sim 28,000$  events is shown in Fig. 1; its main features are the bands associated with the three charge configurations of the  $\rho(770)$ , and the almost complete absence of events near the center of the plot.

### 3. The Amplitude Describing the Decay $J/\psi \rightarrow \rho\pi$ .

The vector coupling of the initial state electron and positron to the  $J/\psi$  implies, to a very good approximation, that the latter is produced only with spin projection (i.e. helicity)  $\pm 1$  along the beam direction. For each  $J/\psi$  helicity configuration, i. the properly-symmetrized amplitude describing decay to  $\rho\pi$  takes the form

$$A_i = A_i^0(\pi^-, \pi^+) + A_i^+(\pi^+, \pi^0) + A_i^-(\pi^0, \pi^-); \quad (2)$$

each superscript denotes the net charge of the dipion system constituting the  $\rho$  in question; the specific dipion configuration is denoted in parentheses, with the convention that the first pion is the one which is used to define the decay angles of the  $\rho$ . The resulting three-pion amplitude is then consistent with the requirements of Bose symmetry, and the intensity distribution for the final state is given by

$$dI = (|A_1|^2 + |A_{-1}|^2) d(LLPS), \quad (3)$$

where  $d(LLPS)$  denotes the relevant element of Lorentz-invariant phase space.

Using, for example, the helicity formalism, it can be shown that the  $A_i^\pm$  (where  $i$  denotes the net charge configuration) take the form

$$A_1^\pm = B(m) \sin\theta_1 (\cos\phi_1 + i \cos\theta_1 \sin\phi_1) e^{i\phi} \quad (4)$$

and

$$A_{-1}^\pm = B(m) \sin\theta_1 (\cos\phi_1 - i \cos\theta_1 \sin\phi_1) e^{-i\phi}; \quad (5)$$

$\theta$  and  $\phi$  are the polar and azimuthal angles of the  $\rho$  in the  $J/\psi$  rest frame (i.e. the lab. frame), while  $\theta_1$  and  $\phi_1$  are the polar and azimuthal angles of the designated decay pion in the  $\rho$  rest frame. The function  $B$  expresses the dependence of the amplitude on the dipion mass,  $m$ , and takes the form

$$B(m) = \frac{p \left( \frac{q}{q_\rho} \right)}{m_\rho^2 - m^2 - im_\rho \Gamma(m)} \quad (6)$$

with

$$\Gamma(m) = \Gamma_\rho \left( \frac{q}{q_\rho} \right)^3 \left( \frac{m_\rho}{m} \right); \quad (7)$$

$m_\rho$  and  $\Gamma_\rho$  correspond to the PDG values of the mass and width of the  $\rho(770)$ ,<sup>[1]</sup>  $p$  is the magnitude of the  $\rho$  three-momentum in the  $J/\psi$  rest frame, while  $q$  is the

magnitude of the three-momentum of the designated decay pion in the  $\rho$  rest frame;  $q_\rho$  is the value of  $q$  for  $m=m_\rho$ . The factors  $p$  and  $q$  in the numerator of equ.(6) result from the P-wave nature of the  $J/\psi$  and  $\rho$  decays, respectively. A P-wave Blatt-Weisskopf barrier factor was also included originally in the description of  $\rho$  decay. However, the fits to be described below clearly require the radius parameter to be zero; consequently, this factor is excluded from eqs. (6) and (7).

Equation (4)-(7) may be incorporated into equ.(2) to express the amplitudes  $A_1$  and  $A_{-1}$  in the full dimensionality of the final state variables; equ.(3) then yields the intensity distribution in this space.

### 4. The Fit to the Data.

Monte Carlo studies of reaction (1) revealed that the shower counter simulation program is unable to reproduce correctly the photon detection efficiency in the vicinity of the barrel shower counter ribs, at the junction of the barrel and end-cap shower counters, and in the region of the end-cap shower counters near the beam-pipe.<sup>[6]</sup> Consequently, prior to attempting fits to the data, these regions of mis-match were removed by cuts on  $\cos\theta_\gamma^*$ , where  $\theta_\gamma^*$  is the polar angle of either final state photon in the lab. frame. These cuts reduced the data sample available for fitting purposes to  $\sim 19,000$  events.

A maximum likelihood procedure was followed in fitting expression (3) to this data sample. Monte Carlo events were generated according to Lorentz-invariant phase space i.e. with an intensity distribution given by

$$dI \sim d(LLPS) \sim p q d m d \cos\theta d \phi d \cos\theta_1 d \phi_1,$$

where the variables are defined as above, and correspond to one of the dipion configurations. The resulting data sample was subjected to the reconstruction and selection procedures applied to the real data, and the surviving events were then used to obtain the normalization integrals required in the evaluation of the likelihood function. The parameters to be fit are the mass of the neutral  $\rho$ , the mass difference between the charged and neutral  $\rho$  ( $\delta$ ), and the width of the  $\rho$ .

The resulting fit yielded reasonably good descriptions of the charged and neutral  $\rho$  peak regions. However, the Dalitz plot corresponding to the fitted intensity distribution showed no depletion at the center (cf. Fig.1); in fact this region was almost uniformly populated at a relatively high density level. Attempts at reducing this population by means of the Blatt-Weisskopf radius parameter discussed previously failed; they resulted in very poor fits to the  $\rho$  peak regions, and still yielded a uniform, if lower density, population at the center of the Dalitz plot.

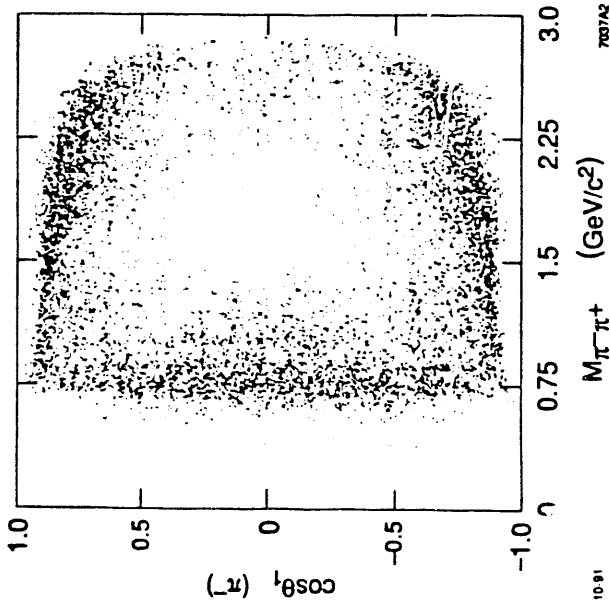


Figure 2. The scatter-plot of  $\pi^- \pi^+$  mass versus  $\cos\theta_1$ , the helicity cosine of the  $\pi^-$  in the  $\pi^- \pi^+$  rest frame.

In order to clarify the reason for this shortcoming, a scatterplot of  $\pi^- \pi^+$  mass versus the helicity cosine ( $\cos\theta_1$ ) of the  $\pi^-$  in the  $\pi^- \pi^+$  rest frame is shown in Fig.2. The curved bands at the top and bottom of the plot are the reflections due to charged  $\rho$  production: selecting the events satisfying  $|\cos\theta_1| \leq 0.2$  almost entirely eliminates contributions from these reflections, so that the resulting mass projection gives a rather clean picture of the mass dependence which is to be described in terms of the function  $B(m)$  of equ.(6).

The data points of Fig.3 represent the superposition of this projection for the three dipion charge configurations; the curve results from equ.(6), and provides a good description of the  $\rho(770)$  peak. However, in the mass range  $\sim 0.9$ - $1.3$   $\text{GeV}/c^2$  the data points are significantly above the extrapolated  $\rho$  line-shape, while in the region above  $\sim 1.4$   $\text{GeV}/c^2$  they exhibit a dramatic drop below the curve; the rise in the data above  $\sim 1.9$   $\text{GeV}/c^2$  is due to reflection from the other  $\rho$  bands (cf. Fig.2). The conclusion to be drawn from Fig.3 is that a parametrization in terms of the  $\rho(770)$  alone is incapable of reproducing the dipion mass dependence of the

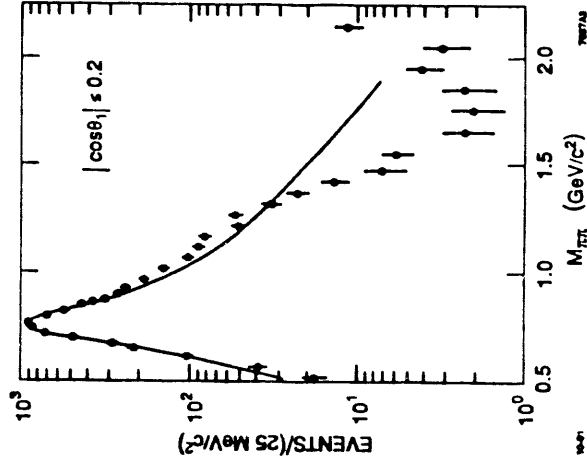


Figure 3. The  $\pi\pi$  mass distribution for  $|\cos\theta_1| \leq 0.2$ ; the distributions for the different dipion charge configurations have been combined; the curve corresponds to the  $\rho$  line-shape, as described in the text.

data on reaction (1).

The mass dependence of Fig.3 is very similar to that of the pion form factor for mass values up to  $\sim 1.6$   $\text{GeV}/c^2$ ,<sup>[7,8]</sup> however, the data of ref.8 have a peak in the region  $1.7$ - $1.8$   $\text{GeV}/c^2$  which is not present in Fig.3. The data of ref.7 are well-described by including the  $\rho(770)$  and significant coherent contributions from two  $J^{PC} = 1^{--}$  excited states of mass  $\sim 1.3$   $\text{GeV}/c^2$  and  $\sim 1.6$   $\text{GeV}/c^2$ . Motivated by this, the data on reaction (1) were re-fit using equ.(6), but with the function  $B$  modified as follows:

$$B(m) = B(m, \rho(770)) + c_1 e^{i\beta_1} B(m, \rho_1(1300)) + c_2 e^{i\beta_2} B(m, \rho_1(1600)). \quad (8)$$

In this expression,  $c_1$ ,  $c_2$ ,  $\beta_1$  and  $\beta_2$  are taken to be constants whose values are the same for all three dipion charge configurations, and which are to be determined by the likelihood fit. The results of the fit indicate that the contribution due to

the  $\rho(1300)$  is small; consequently, the mass and width of this state are fixed at the values obtained in a recent LASS analysis<sup>[6]</sup>, namely 1302 and 140 MeV/c<sup>2</sup>, respectively. The contribution due to the  $\rho(1600)$  proves to be large, and so the mass and width of this state are left free in the fit. It follows that there are nine parameters to be determined, namely  $m_{\rho^0}$ ,  $\delta$ ,  $\Gamma_{\rho^-}$ ,  $m_{\rho}(1600)$ ,  $\Gamma_{\rho}(1600)$ ,  $c_1$ ,  $c_2$ ,  $\beta_1$  and  $\beta_2$ .

The fit yields the following values:

$$\begin{aligned} m_{\rho^0} &= 776.2 \pm 1.3 \text{ MeV}/c^2 \\ \delta &= m_{\rho^+} - m_{\rho^0} = 1.6 \pm 1.5 \text{ MeV}/c^2 \\ \Gamma_{\rho^-} &= 150.6 \pm 2.4 \text{ MeV}/c^2 \\ m_{\rho}(1600) &= 1600 \pm 28 \text{ MeV}/c^2 \\ \Gamma_{\rho}(1600) &= 383 \pm 25 \text{ MeV}/c^2 \\ \beta_1 &= (200 \pm 42)^\circ \\ \beta_2 &= (-120 \pm 8)^\circ \end{aligned}$$

the errors are purely statistical. Under the assumption that the  $J/\psi$  coupling to  $\rho\pi$  is independent of the particular  $\rho$  state involved, the constants  $c_1$  and  $c_2$  can be re-expressed in terms of the elasticity of each state. This gives

$$\sqrt{x_{\rho}(770)} : \sqrt{x_{\rho}(1300)} : \sqrt{x_{\rho}(1600)} = 1 : 0.031 \pm 0.016 : 0.508 \pm 0.017$$

where  $x$  denotes the elasticity i.e. the elasticities are approximately in the ratio 1 : 0.03 : 0.25.

## 5. Discussion of the Fit Results.

The quality of the likelihood fit is illustrated by Figs.4-6; in each figure the points correspond to the data sample on reaction (1), and the histogram is obtained by weighting the Monte Carlo events used to calculate the normalization integrals, by expression (3) evaluated using the fitted values of the parameters. The sum of these Monte Carlo weights is normalized to the number of events in the data sample i.e.19,380 (cf.Fig.4); in this regard, it should be noted that there is no renormalization in Fig.5 and Fig.6, which correspond to much smaller subsets of

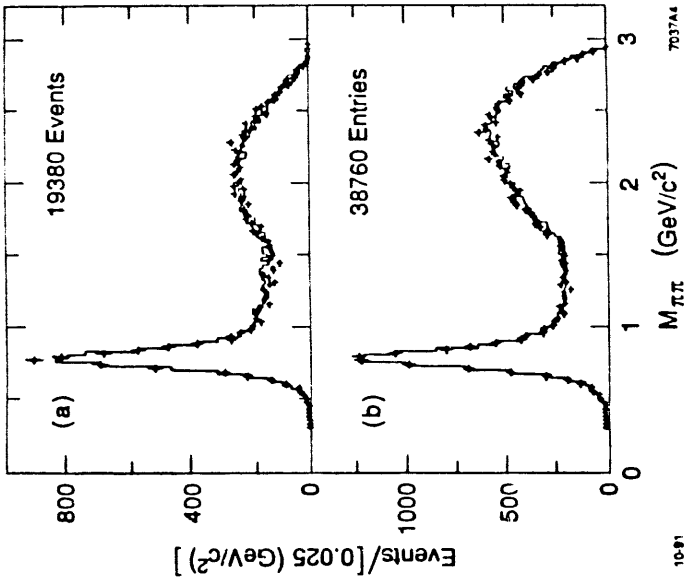


**Figure 4.** (a) The  $\pi^-\pi^+$ , and (b) the combined charged dipion mass distribution for the fit sample for reaction (1) (data points); in each figure the histogram corresponds to the fitted amplitude as explained in the text.

the data and Monte Carlo events. In Fig.4(b) and Fig.5(b) the data on the two charged dipion configurations are added together, while in Fig.6 the data from all three dipion systems are combined. It is clear that in each of Figs.4-6 the shape and absolute normalization of the mass distribution are well reproduced by the weighted Monte Carlo events. In particular, the fact that the dip in Fig.6 is quite well modelled means that the fit reproduces the observed depopulation at the center of the Dalitz plot (cf. Fig.1).

The values of the  $\rho(770)$  width and charged-neutral mass difference are consistent with the PDG values,<sup>[5]</sup> however the mass value differs significantly from that quoted in this reference, namely  $768.7 \pm 0.7$  MeV/c<sup>2</sup>. It should be noted that

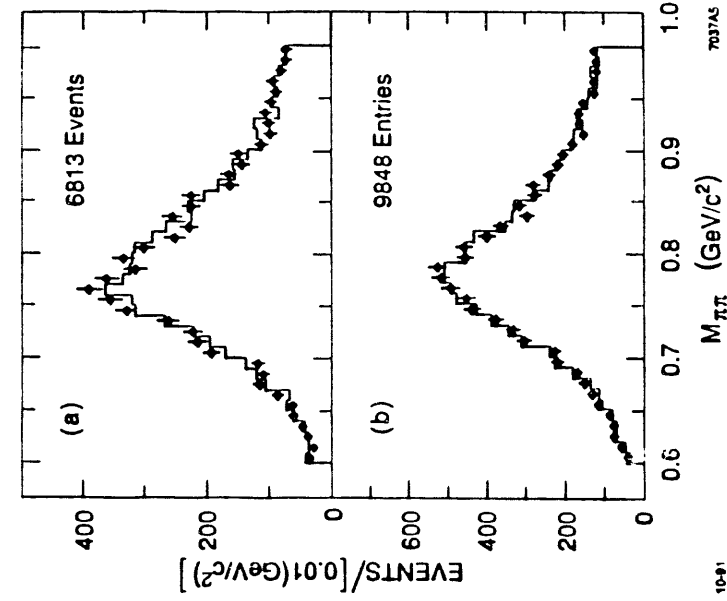


**Figure 5.** The  $\rho$  peak regions of Figs.4(a) and 4(b) in 10  $\text{MeV}/c^2$  mass bins.

the value obtained in the present analysis agrees very well with the high statistics results of Barkov et al.<sup>[7]</sup> ( $775.0 \pm 1.1 \text{ MeV}/c^2$ ) and Hyams et al.<sup>[10]</sup> ( $778. \pm 2 \text{ MeV}/c^2$ ).

The mass, width and elasticity estimate for the  $\rho_1(1600)$  are in good agreement with the results from  $\pi\pi$  scattering phase shift analyses.<sup>[11]</sup> In ref. 11 it is concluded that the preferred P-wave solution contains a resonance of mass  $\sim 1575 \text{ MeV}/c^2$ , width  $\sim 340 \text{ MeV}/c^2$  and elasticity in the range 15-30%, all of which are in accord with the present results. However, the estimate of the elasticity of the  $\rho_1(1300)$  is much lower than the value  $\sim 5\%$  obtained in the LASS analysis.<sup>[6]</sup> This suggests that the coupling of the  $J/\psi$  to this state may be much weaker than that to the

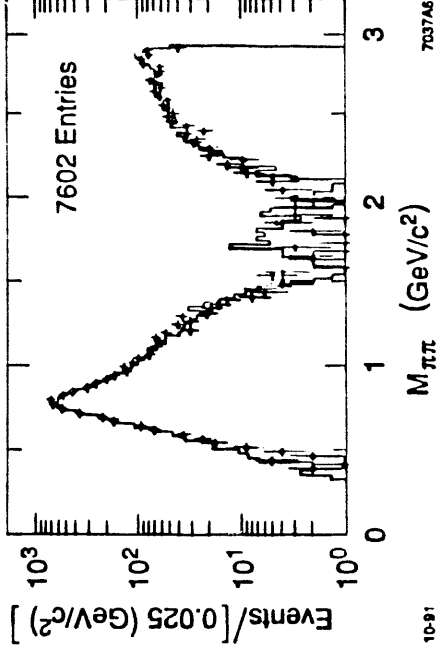


**Figure 6.** The  $\pi\pi$  mass distribution for the events in the analysis sample satisfying  $|\cos\theta_1| \leq 0.2$  (data points); the distributions for the different dipion charge configurations have been combined; the histogram corresponds to the fit described in the text.

$\rho(770)$  or to the  $\rho_1(1600)$ .

The data of Bisello et al.<sup>[6]</sup> on the pion form factor seem to require a fourth  $\rho$  state of mass  $\sim 1720 \text{ MeV}/c^2$ . Preliminary indications are that the inclusion of such a state in the fit to reaction (1) leads to an improved fit to the dip in Fig.6, and a better description of the central region of the Dalitz plot. This result, together with the values of all relevant branching fractions, will appear in a future publication containing the final results of the analysis.

In the context of the quark model, the most likely interpretation of the  $\rho_1(1600)$  is that it is a partner of the  $\rho_3(1690)$  in the D-wave ground state triplet i.e. it is the  $1^3D_1$  state. The much lower mass and small elasticity of the  $\rho_1(1300)$  suggest that this state may be the first radial excitation of the  $\rho(770)$  i.e. it is the  $2^3S_1$  state. Similarly, if there is indeed a fourth state at  $\sim 1.7 \text{ GeV}/c^2$ , its mass and weak coupling to  $J/\psi$  suggest that it might be the second radial excitation of the  $\rho(770)$  i.e. the  $3^3S_1$  state. However, these assignments may constitute an oversimplification in the sense that the  $^3S_1$  and  $^3D_1$  states can mix in principle, so that the observed states may not be in one-to-one correspondence with the pure quark model states.

## 6. Conclusion.

The present analysis has shown that it is possible to obtain a complete description of the data on reaction (1) in terms of a properly symmetrized amplitude representing the sequential two-body decays  $J/\psi \rightarrow \rho\pi$  and  $\rho \rightarrow \pi\pi$ . However, the absence of events at the center of the Dalitz plot (Fig.1) requires that the  $J/\psi$  couple strongly to the  $\rho_1(1600)$  as well as to the  $\rho(770)$ ; the  $J/\psi$  also seems to couple weakly to the  $\rho_1(1300)$ , and perhaps also to a fourth  $\rho_1$  state of mass  $\sim 1.7$  GeV/ $c^2$ .

The mass of the  $\rho(770)$  obtained from the fit to reaction (1) disagrees with the present World Average,<sup>[1]</sup> but is in good agreement with other high statistics measurements of the  $\pi\pi$  P-wave amplitude.<sup>[7,10]</sup> The mass, width and estimated elasticity of the  $\rho_1(1600)$  are consistent with the values obtained from  $\pi\pi$  elastic scattering phase shift analyses.<sup>[11]</sup>

In terms of the quark model level structure, the  $\rho_1(1600)$  may be the  $^3D_1$  ground state, while the  $\rho_1(1300)$  and  $\rho_1(\sim 1700)$  may correspond to the first and second radial excitations of the  $\rho(770)$ . However, to the extent that these states may mix, this interpretation may be a gross over-simplification.

## REFERENCES

1. Review of Particle Properties, Particle Data Group, Phys. Lett. **B 239** (1990) 1.
2. K. F. Einsweiler, Ph.D thesis, Stanford University, (1984), unpublished.
3. R. M. Baltrusaitis *et al.*, Phys. Rev. **D 32** (1985) 2883.
4. R. M. Baltrusaitis *et al.*, Phys. Rev. **D 35** (1987) 2077.
5. T. A. Bolton, Ph.D thesis, Massachusetts Institute of Technology, (1988), unpublished.
6. D. Bernstein *et al.*, NIM **226** (1984) 301.
7. L. M. Barkov *et al.*, Nucl. Phys. **B 256** (1985) 365.
8. D. Bisello *et al.*, Phys. Lett. **B 220** (1989) 321.
9. D. Aston *et al.*, SLAC PUB-5657 (1991).
10. B. Hyams *et al.*, Nucl. Phys. **B 64** (1973) 134.
11. A. D. Martin and M. R. Pennington, Ann. Phys. **114** (1978) 1.

**END**

**DATE  
FILMED**

*01/09/91*

